Available online at www.sciencedirect.com
SCIENCE DIRECT®
International Journal of Thermal Sciences 44 (2005) 21–32
International Journal of Thermal Sciences
www.elsevier.com/locate/ijts

Flow, thermal, and entropy generation characteristics inside a porous channel with viscous dissipation

Shohel Mahmud *, Roydon Andrew Fraser

Department of Mechanical Engineering (E3-2136C), University of Waterloo, 200 University Avenue West, Waterloo, Ontario N2L3G1, Canada

Received 6 November 2003; received in revised form 4 May 2004; accepted 5 May 2004

Available online 21 August 2004

Abstract

We present both analytical and numerical analyses of fully developed forced convection and entropy generation in a fluid-saturated porous medium channel bounded by two parallel plates. The flow in the porous material is described by the Darcy–Brinkman momentum equation. Differentially heated isothermal walls are selected as thermal boundary conditions. Analytical expressions for velocity, temperature, Nusselt number, entropy generation rate, and heat transfer irreversibility are obtained after simplifying and solving the governing differential equations with reasonable approximations. Subsequent results obtained by numerical calculations show excellent agreement with analytical results.

Keywords: Darcy number; Energy streamline; Entropy generation; Thermoacoustics; Viscous dissipation

1. Introduction

The study of convection processes in porous media is a well-developed field of investigation because of its importance to a variety of situations. For example, thermal insulation, geothermal system, solid matrix heat exchangers, nuclear waste disposal, microelectronic heat transfer equipment, coal and grain storage, petroleum industries, and chemical catalytic beds. The literature on the topic of forced convection and free convection in porous media is well surveyed by Nield and Bejan [1] and Bejan [2]. Another potential application of convection processes in porous media is found in thermoacoustic prime movers and heat pumps (Swift [3]). Our primary goal is to incorporate into the fundamental thermoacoustics theory of Swift [3] and Rott [4] a modification that treats the fluid-gap within stacks of a thermoacoustic engine/refrigerator as porous media. Thermoacoustic engines are devices which make use of the thermoacoustic phenomena and function as heat pumps or prime movers. They can provide cooling or heating using environmentally benign gases as the working fluid. Despite recent developments in thermoacoustic engines (see Swift [3]), there are many areas requiring further investigation in order to better predict their performance and guide future designs for thermoacoustic engines. Any thermoacoustic device (system) can be divided into four basic components (resonant tube, speaker, heat exchangers, and regenerator or stacks); among them the stack serves as the heart of the thermoacoustic device. In engines and heat pump, stacks are finely subdivided into many parallel channels or pores. Starting from the single plate, stacks are available in different sizes and shapes. Multi-plate arrays, honeycombs, spiral roles, and pin arrays' are some example of stacks commonly used in thermoacoustic engines and refrigerators (see Swift [1]). To improve the thermal contact and heat transfer area, a porous medium (a fine wire mesh made of a material with moderate to good thermal conductivity) of moderate permeability may be embedded inside the fluid gap between two consecutive stacks. Most of the existing theories (of thermoacoustic engines/prime movers) consider a non-porous medium and very few of them use a single pore

* Corresponding author.
E-mail address: smahmud@engmail.uwaterloo.ca (S. Mahmud).

1290-0729/$ – see front matter
doi:10.1016/j.ijthermalsci.2004.05.001

Nomenclature

a_0	inverse of the square root of the Darcy number, $=1/\sqrt{Da}$	T_{hot}	temperature of the hot wall ..... °C
C_m	constants of integration, $m=1, 2, 3$, and 4.	T_{cold}	temperature of the cold wall ..... °C
C_p	specific heat of the fluid at constant pressure ..... $kJ{\cdot}kg^{-1}{\cdot}°C^{-1}$	u	dimensionless axial velocity
Da	Darcy number, $=K/w^2$	u^*	axial velocity inside the channel ..... $m{\cdot}sec^{-1}$
$\dot{E}$	energy flux density vector ..... $W{\cdot}m^{-2}$	v	dimensionless transverse velocity
Ec	Eckert number	v^*	transverse velocity ..... $m{\cdot}sec^{-1}$
h	convective heat transfer coefficient ..... $W{\cdot}m^{-2}{\cdot}°C^{-1}$	w	half width of a channel ..... m
K	permeability of the porous media ..... m^2	*Greek symbols*	
k_f	thermal conductivity of the fluid $W{\cdot}m^{-1}{\cdot}°C^{-1}$	α_f	thermal diffusivity of the fluid ..... $m^2{\cdot}sec^{-1}$
L	length of the channel ..... m	ε	porosity of the porous medium
Nu	Nusselt number, $=hw/k_f$	μ	dynamic viscosity of the fluid..... Pa·sec
p	dimensionless pressure	ν	kinematic viscosity of the fluid..... $m^2{\cdot}sec^{-1}$
p^*	pressure..... Pa	Φ	pressure gradient parameter, $=(\partial p/\partial x)\times Re$
Re	Reynolds number	Ω	dimensionless temperature difference
T	temperature of the fluid ..... °C	Θ	dimensionless temperature
		τ	dimensionless time
		ρ	density of the fluid ..... $kg{\cdot}m^{-3}$

(of circular or square cross-section) to model thermoacoustic systems. To model a thermoacoustic problem, it is necessary to solve the unsteady-compressible-viscous Navier–Stokes equation at very low Mach number along with the energy equations in the fluid region and solid walls. Such modeling is one of the most complicated and challenging fluid dynamics problems, to which very few solutions exist. Only a few restricted 1-D cases are known (Rott [4] and Swift [5]). In developing a thermoacoustic theory that incorporates porous media, a step by step development is required; starting from the simplest possible case (steady-incompressible problem in porous media), proceeding to the complicated (unsteady-compressible-conjugate problem in porous media). In this paper, we only focus on steady-state, incompressible flow in porous media bounded by two parallel plates of negligible thickness. The unsteady, compressible, version of this problem with conjugate effects is left for future work.

In thermoacoustic devices, stacks are repeated along the transverse direction of fluid motion. The fluid gap between two consecutive stacks is usually kept constant. Two consecutive stack plates and the fluid gap may be approximated as a *unit-channel* and inside the resonant chamber the stack (or regenerator) consists of many *unit-channels*. The fluid dynamics of all *unit-channels* must be similar (neglecting resonant chamber wall effects). Therefore, for simplicity, we consider one *unit-channel* for the present investigation. Kaviany [6] presented an analytical solution to the transport equations based on the Brinkman-extended Darcy flow model. For an isothermal boundary condition, Kaviany [6] reported an increasing Nusselt number with increasing porous media shape parameter ($=\sqrt{\varepsilon}/Da$) for fully developed flow. Assuming a boundary layer type developed flow, Vafai and Kim [7] presented a closed form solution to the Brinkman–Forchheimer-extended Darcy momentum equation and the associated heat transfer equation for the case of fully developed flow with uniform heat flux at the boundaries. Nield et al. [8] theoretically analyzed fully developed forced convection in a fluid-saturated porous-medium channel bounded by parallel plates, with imposed uniform heat flux or isothermal conditions at the plates. They included the non-linear Forchheimer term in the momentum equation and reported an exact solution. For a special type of porous medium (packed bed of spheres), Poulikakos and Renken [9] reported a numerical study of convective transport characteristics. Subsequent experimental results by Renken and Poulikakos [10] agreed with the predictions of Poulikakos and Renken [9]. Other examples of exact and approximate solutions for the forced convection problem are available in Nakayama et al. [11]. Nield et al. [12,13] selected an analysis method close to the classical Graetz analysis method in order to investigate thermally developing forced convection problems in porous media in a parallel-plate channel or circular duct. They assumed a large Péclet number and neglected the longitudinal conduction effect. Nield et al. [14] extended the work of Nield et al. [12,13] by including longitudinal conduction and viscous dissipation effects using a modified Graetz methodology. Some other effects, for example, the effect of a localized heat source was studied by Hadim [15], Sun et al. [16], and Cui [17]; the effect of local thermal non-equilibrium was by Nield [18] and Nield and Kuznetsov [19]; and, the effect of non-Newtonian fluid flow was studied by Chen and Hadim [20].

The foregoing discussions that deal with the forced convection problem at different flow-thermal situations and boundary conditions in porous channels are very much restricted to First-Law (of thermodynamics) analyses. None

of the above works performed a Second-Law based analysis to determine the nature of the irreversibility in terms of entropy generation. For a real system the generated entropy is proportional to the destroyed exergy (Bejan [21]). Exergy is always destroyed, partially or totally: this is a consequence of the Second-Law of thermodynamics. The destroyed exergy or the generated entropy is responsible for the less-than-theoretical maximum thermodynamic efficiency of a system. Through exergy accounting in smaller and smaller subsystems (total system → components → elemental surfaces → differential levels, etc.), we are able to draw a map of how the destruction of exergy is distributed over the engineering system of interest (Bejan [22]). In this way we are able to pinpoint the components and mechanisms (processes) that destroy the most exergy. This knowledge offers a real advantage in the search to improve system efficiency, because it tells us from the start how to allocate engineering effort and resources. The exergy-based method is fundamentally different from the traditional, much more popular, energy-based techniques (Bejan et al. [23]), used for analysis in the heat transfer community. One attribute of an exergy-based analysis is that it makes it possible to compare on a common basis (entropy generation platform) different interactions (inputs, outputs, work transfer, heat transfer, etc.) in a system thus enabling a minimization of the global entropy generation rate (entropy generation minimization or EGM).

In the view of the above, this study examines the flow, thermal, and entropy generation fields inside a parallel-plate porous channel when subjected to differentially heated isothermal walls. The governing flow and energy equations are first simplified and solved to obtain analytical solutions that include viscous dissipation effects. A numerical simulation is also conducted using a control volume approach. The resulting velocity and temperature profiles, Nusselt number, entropy generation rate, and Bejan numbers' variation are investigated as a function of Darcy number.

2. Mathematical formulation

The analysis is carried out for a steady-state, incompressible, two-dimensional flow within a parallel-plate channel filled with a homogeneous and isotropic porous medium, and heated with uniform wall temperatures. The porous medium is saturated with a single phase Newtonian fluid and is assumed to be in local thermodynamic equilibrium with the fluid. The thermophysical properties of the solid matrix and of the fluid are assumed to be constant. Although for certain porous media such as packed beds the porosity may vary due to channeling near the walls (Vafai and Kim [24]), in the present study, a fibrous or wire-mesh-metal material is considered such that the porosity and permeability are assumed to be constant even close to the walls (Hunt and Tien [25]). Natural convection and thermal radiation effects are neglected. Viscous dissipation is included in the energy equation. The non-dimensional governing equations can be written as

$$\frac{\partial u}{\partial x}+\frac{\partial v}{\partial y}=0 \tag{1}$$

$$u\frac{\partial u}{\partial x}+v\frac{\partial u}{\partial y}=-\frac{\partial p}{\partial x}+\frac{1}{Re}\left(\frac{\partial^2 u}{\partial x^2}+\frac{\partial^2 u}{\partial y^2}\right)-\frac{1}{Re\,Da}u \tag{2}$$

$$u\frac{\partial v}{\partial x}+v\frac{\partial v}{\partial y}=-\frac{\partial p}{\partial y}+\frac{1}{Re}\left(\frac{\partial^2 v}{\partial x^2}+\frac{\partial^2 v}{\partial y^2}\right)-\frac{1}{Re\,Da}v \tag{3}$$

$$u\frac{\partial \Theta}{\partial x}+v\frac{\partial \Theta}{\partial y}=\frac{1}{Re\,Pr}\left(\frac{\partial^2 \Theta}{\partial x^2}+\frac{\partial^2 \Theta}{\partial y^2}\right)+\frac{Ec}{Re\,Da}\left(u^2+v^2\right) \tag{4}$$

In Eqs. (1) to (4), the different variables and non-dimensional numbers are defined as

$$x=\frac{x^*}{w},\qquad y=\frac{y^*}{w},\qquad u=\frac{u^*}{u_0},\qquad v=\frac{v^*}{u_0}$$

$$p=\frac{p^*}{\rho u_0^2},\qquad \Theta=\frac{T-T_c}{T_h-T_c}$$

$$Re=\frac{\rho w u_0}{\mu},\qquad Da=\frac{K}{w^2}$$

$$Ec=\frac{u_0^2}{C_p\Delta T},\qquad Pr=\frac{\mu C_p}{k_f} \tag{5}$$

Eqs. (1)–(4) are non-linear in nature and analytical solutions are not possible to these equations. However, with some restrictions, a simplification is possible for Eqs. (1)–(4) and in that situation a closed from of solutions are possible. In the next sections, analytical solutions are presented for the simplified equations. Results obtained by numerical calculation for the full equations are given in a later sections. The description of the numerical methodology used is given in Mahmud et al. [26] and is not repeated here.

3. Flow and thermal field

In this section, our primary goal is to select a situation where an analytical solution is possible. Therefore, we exclude the inlet and exit regions from our analysis and focus on the portion of the channel where flow and thermal

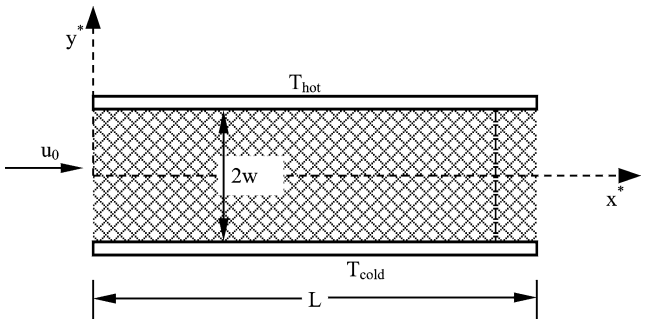

Fig. 1. Schematic diagram of the problem.

fields are hydrodynamically and thermally developed. For the steady-state hydrodynamically developed situation we have unidirectional flow in the x^*-direction between impermeable boundaries at $y^* = w$ and $y^* = -w$, as illustrated in Fig. 1. The unidirectional flow assumption implies, $v = 0$, and with the help of continuity equation, that the '$\partial u/\partial x$' term will be zero. Based on these assumptions and simplifications, the axial momentum equation reduces to

$$\frac{\partial^2 u}{\partial y^2} + \frac{1}{Da}u = -Re\left(\frac{\partial p}{\partial x}\right) \tag{6}$$

where *Da* and *Re* are the Darcy and Reynolds numbers, respectively. The general solution to Eq. (6) is

$$u = C_1 \sinh\left(\frac{y}{\sqrt{Da}}\right) + C_2 \cosh\left(\frac{y}{\sqrt{Da}}\right) - Da\,Re\left(\frac{\partial p}{\partial x}\right) \tag{7}$$

where C_1 and C_2 are two constants of integration. Applying the boundary conditions: (a) no slip, i.e., $u(y = 1) = 0$ or $u(y = -1) = 0$ and (b) symmetry, i.e., $(\partial u/\partial y)_{y=0} = 0$, the final expression for velocity becomes

$$u = -Da\,Re\left(\frac{\partial p}{\partial x}\right)\left[1 - \frac{\cosh(y/\sqrt{Da})}{\cosh(1/\sqrt{Da})}\right] \tag{8}$$

Therefore, the fully developed axial velocity depends on the Darcy number (*Da*), Reynolds number (*Re*), and axial pressure gradient ($\partial p/\partial x$). Darcy number (*Da*) is a measure of the relative permeability of the porous media and is frequently found in problems that include a non-Darcy model for the porous media. In the limit of a very large Darcy number ($Da \to \infty$), the expression of velocity (Eq. (8)) reduces to

$$u_\infty = \lim_{Da\to\infty}(u) = -\frac{1}{2}Re\left(\frac{\partial p}{\partial x}\right)(1 - y^2) \tag{9}$$

which is similar to the expression obtained in plane Poiseuille flow [27]. The expression for average velocity is

$$u_{av} = -Da\,Re\left(\frac{\partial p}{\partial x}\right)\left[1 - \frac{\sinh(1/\sqrt{Da})}{\cosh(1/\sqrt{Da})}\right] \tag{10}$$

Usually, in this type of flow situation, the pressure gradient term is a constant which means that pressure varies linearly along the axial distance of the channel. Numerical calculations show that the product of *Re* and $\partial p/\partial x$ is approximately constant for *Da* greater than 3.0 as long as the flow is laminar. Expressing the product of *Re* and $\partial p/\partial x$ as a new parameter Φ, the behavior of Φ as a function of Darcy number is shown in Fig. 2. For $Da < 0.3$, the magnitude of Φ drops linearly on a log–log plot with increasing *Da*. A power curve, defined by the relation $\Phi = 1.54033 \times Da^{-0.93327}$, is best suited for describing the $\Phi - Da$ behavior for $Da < 0.3$. For $Da > 3.0$, Φ changes less than 0.1% with increasing Darcy number as it asymptotes to 2.95. For the small range of Darcy number, $0.3 \leqslant Da \leqslant 3.0$, the hyperbolic fit defined by the relation $\Phi = 2.95 + 1.1539 \times Da^{-1}$, works well (maximum error is 1%). Alternatively, the following fourth order polynomial is valid for describing the $\Phi - Da$ relationship in a less accurate manner (±7%) for the range $10^{-3} \leqslant Da \leqslant 10^3$:

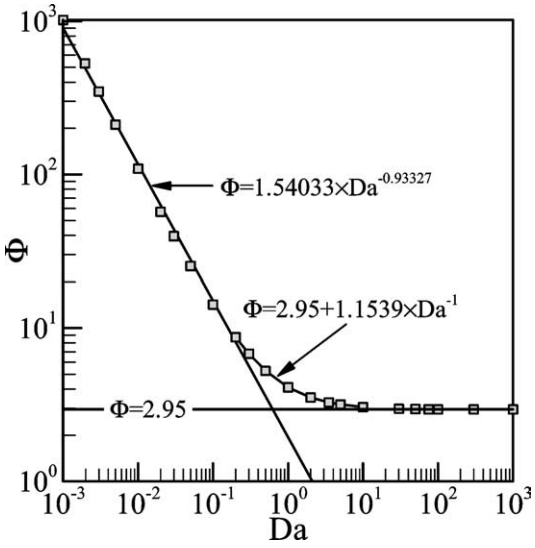

Fig. 2. Variation of Φ as a function of Darcy number.

$$\Phi_0 = a_1 + a_2 Da_0 + a_3 Da_0^2 + a_4 Da_0^3 + a_1 Da_0^4 \tag{11}$$

where

$$\Phi_0 = \log_{10}(\Phi), \qquad Da_0 = \log_{10}(Da)$$
$$a_1 = 0.6286371, \qquad a_2 = -0.34693803$$
$$a_3 = 0.118506167, \qquad a_4 = -0.0090305076$$
$$a_5 = -0.006993169$$

An alternate, non-dimensional, way of expressing the velocity is

$$U = \frac{u}{u_{av}} = \frac{\cosh(y/\sqrt{Da}) - \cosh(1/\sqrt{Da})}{\sqrt{Da}\sinh(1/\sqrt{Da}) - \cosh(1/\sqrt{Da})} \tag{12}$$

Eq. (12) free from any influence of Φ and is a function of Darcy number only. Based on the same assumptions already used in this work, the simplified form of the energy equation (Eq. (4)) is

$$\frac{\partial^2 \Theta}{\partial y^2} + \frac{Ec\,Pr}{Da}u^2 = 0 \tag{13}$$

where *Ec* and *Pr* are the Eckert and Prandtl numbers, respectively. This simplified form of the energy equation (Eq. (13)) expresses a balance between two possible effects: transverse conduction and viscous dissipation. The modeling of the viscous dissipation term is a controversial issue. Nield [28] argued that the viscous dissipation term should remain to the power of the drag force when the Brinkman equation is considered, and in that case the dimensional viscous dissipation term becomes

$$\text{viscous dissipation} = \frac{\mu(u^*)^2}{K} - \mu_{\text{eff}}u^*\frac{\partial^2 u^*}{\partial y^{*2}} \tag{14}$$

On the other hand, Al-Hadhrami et al. [29] proposed an alternate expression for the viscous dissipation term derived

from the Navier–Stokes equation for a fluid clear of solid material in the case of large Darcy number; and in this case the expression becomes

$$\text{viscous dissipation} = \frac{\mu(u^*)^2}{K} + \mu\left(\frac{\partial u^*}{\partial y^*}\right)^2 \tag{15}$$

However, in this paper, we consider only the first term of Eqs. (14) or (15) similar to Bejan [30] in order to make the analysis simple. Plans are to include Eqs. (14) and (15) in a later work. The general solution to Eq. (13) is then

$$\Theta = -Ec\,Pr\,Da\,\Phi^2\left[\frac{y^2}{2} - \frac{2Da\cosh(y/\sqrt{Da})}{\cosh(1/\sqrt{Da})} + \frac{Da\cosh^2(y/\sqrt{Da}) + y^2}{4\cosh^2(1/\sqrt{Da})}\right] + C_3 y + C_4 \tag{16}$$

Applying the boundary conditions: (a) isothermal hot wall, i.e., $\Theta(y=1)=1$ and (b) isothermal cold wall, i.e., $\Theta(y=-1)=0$, the integration constants, C_3 and C_4, become

$$C_3 = \frac{1}{2}$$

$$C_4 = Ec\,Pr\,Da\,\Phi^2\left[\frac{1}{2} - \frac{7Da}{4} + \frac{1}{4\cosh^2(1/\sqrt{Da})}\right] \tag{17}$$

In the limit of a very large Darcy number ($Da \to \infty$), the expression for dimensionless temperature (Eq. (16)) reduces to

$$\Theta_\infty = \lim_{Da\to\infty}(\Theta) = \frac{1}{2}(1+y) \tag{18}$$

which is linear and therefore a conduction like temperature distribution. Using the following definition of Nusselt number

$$Nu = \frac{hw}{k_f} = \left(\frac{w}{T_{\text{hot}} - T_{\text{cold}}}\right)\frac{\partial T}{\partial y^*}\Big|_{y^*=w} = \frac{\partial\Theta}{\partial y}\Big|_{y=1} \tag{19}$$

and using Eqs. (16), (17) and (19), an expression for Nusselt number is obtained in the following form

$$Nu = -Ec\,Pr\,Da\,\Phi^2\left[\frac{3\sqrt{Da}}{2}\tanh\left(\frac{1}{\sqrt{Da}}\right) - \frac{1}{2}\operatorname{sech}^2\left(\frac{1}{\sqrt{Da}}\right) - 1\right] + \frac{1}{2} \tag{20}$$

Eq. (20) is a function of Eckert number, Prandtl number, Darcy number, and Φ. In the limit of very large Darcy number ($Da \to \infty$), Eq. (20) simplifies to a value 0.5;

$$Nu_\infty = \lim_{Da\to\infty}(Nu) = \frac{1}{2} \tag{21}$$

The trailing constant term of 1/2 in the expression for Nu is equivalent to Nu_∞, therefore Nu_∞ can be used to define a modified Nusselt number (Nu^*) in the following form

$$Nu^* = \frac{Nu - Nu_\infty}{Ec\,Pr\,\Phi^2} = -Da\left[\frac{3\sqrt{Da}}{2}\tanh\left(\frac{1}{\sqrt{Da}}\right) - \frac{1}{2}\operatorname{sech}^2\left(\frac{1}{\sqrt{Da}}\right) - 1\right] \tag{22}$$

The modified Nusselt number is a function of Darcy number only.

4. Entropy generation

The convection process in a channel is inherently irreversible. Non-equilibrium conditions arise due to the exchange of energy and momentum within the fluid and at the solid boundaries. This causes continuous entropy generation. One portion of this entropy production is due to heat transfer in the direction of finite temperature gradients. Finite temperature difference heat transfer irreversibly is common in all types of thermal engineering applications. Another portion of the entropy production arises due to fluid friction irreversibility. For 2-D flow though a porous channel, the dimensionless form of entropy generation (Tasnim et al. [31]) is given by

$$Ns = \left\{\left(\frac{\partial\Theta}{\partial x}\right)^2 + \left(\frac{\partial\Theta}{\partial y}\right)^2\right\} + n\frac{Br}{\Omega}\left[2\left(\frac{\partial u}{\partial x}\right)^2 + 2\left(\frac{\partial v}{\partial y}\right)^2 + \left(\frac{\partial u}{\partial y} + \frac{\partial v}{\partial x}\right)^2\right] + (1-n)\frac{Br^*}{\Omega}\left(u^2+v^2\right) \tag{23}$$

where Ns, Br, Br^*, and Ω are entropy generation number, Brinkman number, modified Brinkman number, and dimensionless temperature difference, respectively. These parameters are defined by

$$Ns = \frac{\dot{S}'''_{\text{gen}}}{S_0}, \qquad S_0 = \frac{k_f(\Delta T)^2}{w^2 T_0^2}$$

$$Br = Ec\,Pr, \qquad Br^* = \frac{Br}{\sqrt{Da}}, \qquad \Omega = \frac{\Delta T}{T_0} \tag{24}$$

The index n in Eq. (23) is set equal to 1 for a non-Darcy model of the porous media. For a channel with a porous media that obeys Darcy's model n is set equal to 0. Using the same assumptions already used to simplify the momentum and energy equations, the simplified version of the entropy generation equation is

$$Ns = \left(\frac{\partial\Theta}{\partial y}\right)^2 + n\frac{Br}{\Omega}\left(\frac{\partial u}{\partial y}\right)^2 + (1-n)\frac{Br^*}{\Omega}u^2 \tag{25}$$

By substituting Eqs. (8) and (16) into Eq. (25), the expression for entropy generation number becomes

$$Ns = \left[-G_T\left\{y - \frac{3\sinh(a_0 y)}{2a_0\cosh(a_0)} + \frac{1}{2\cosh^2(a_0)}\right\} + \frac{1}{2}\right]^2 + n\frac{G_u^2 Br\,a_0^2\sinh^2(a_0 y)}{\Omega\cosh^2(a_0)} + (1-n)G_u^2\frac{Br^*}{\Omega}\left\{1 - \frac{\cosh(a_0 y)}{\cosh(a_0)}\right\}^2 \tag{26}$$

where $G_T = Ec\,Pr\,Da\,\Phi^2$, $G_u = Da\,\Phi$, $a_0 = \frac{1}{\sqrt{Da}}$. The entropy generation number (Ns) is also a measure of the total irreversibility of a system. Heat transfer's contribution to total entropy generation rate can be measured by the Bejan number (Be), which is a ratio of the heat transfer irreversibility (HTI) to the total entropy generation rate (Ns). The heat transfer irreversibility can be calculated from

$$\mathrm{HTI} = \left[-Ec\,Pr\,Da\,\Phi^2 \left\{ y - \frac{3\sinh(a_0 y)}{2a_0\cosh(a_0)} + \frac{1}{2\cosh^2(a_0)} \right\} + \frac{1}{2} \right]^2 \tag{27}$$

In the limit of very large Darcy number ($Da \to \infty$), the expression for entropy generation number (Ns) reduces to the following forms:

$$n = 0: \quad Ns_\infty = \frac{Br^*\Phi^2}{4\Omega}\left(1 - y^2 + y^4\right) + \frac{1}{4}$$
$$n = 1: \quad Ns_\infty = \frac{Br}{\Omega}\Phi^2 y^2 + \frac{1}{4} \tag{28}$$

Also for $Da \to \infty$, the Bejan number reduces to the following forms:

$$n = 0: \quad Be_\infty = \left[1 + \frac{Br^*}{\Omega}\Phi^2\left(1 - 2y^2 + y^4\right)\right]^{-1}$$
$$n = 1: \quad Be_\infty = \left(1 + 4\frac{Br}{\Omega}\Phi^2 y^2\right)^{-1} \tag{29}$$

5. Results and discussion

5.1. Flow field

The dimensionless form of the velocity (Eq. (12)) is plotted in Fig. 3 as a function of dimensionless transverse distance (y). Six different Darcy numbers are selected including two limiting extremes, i.e., $Da \to 0$ and $Da \to \infty$. Results obtained from numerical calculation are also presented for the same range of Darcy number and shown by square symbols in Fig. 3. For a negligible Darcy number ($Da \to 0$), the velocity profile is independent of the transverse distance y and slip flow occurs at the walls. Several authors have obtained the slip flow solution before, for example, Nield and Kuznetsov [19]. However, an increasing Darcy number increases the permeability inside the channel, thus leading to a non-linear distribution of velocity as shown in Fig. 3. A high near wall velocity gradient and flat velocity distribution around the centerline of the channel characterize the flow for $Da = 0.01$. The flatness of the velocity profile diminishes with increasing Darcy number. When Da approaches a very large value ($Da \to \infty$), the velocity profile approaches a shape similar to that seen in plane Poiseuille flow (White [27]). Recall from Eq. (12) that Darcy number alone controls the shape of the velocity profile. With the flat portion of the velocity profile extending further towards the solid wall as Da decreases, shorter entrance length is expected as Da decreases. In effect, the boundary layer thickness decreases as Da decreases.

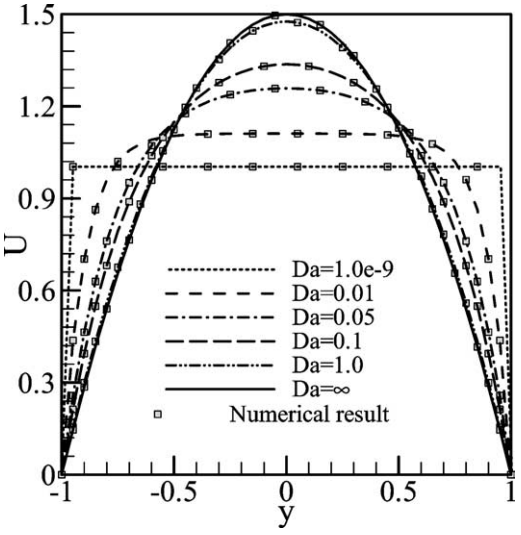

Fig. 3. Velocity as a function of transverse distance at different Da.

5.2. Thermal filed

Fig. 4(a) and (b) show the dimensionless temperature (Θ) distribution as a function of transverse distance (y) for different Darcy numbers. Again, square symbols represent the corresponding values of Θ obtained from numerical calculation. The numerical calculations considered three different forms of the energy equation: an energy equation with (a) conduction and dissipation terms (case 1), (b) conduction, convection, and dissipation terms (case 2), and (c) conduction and convection terms (case 3). These three cases are considered with the intention to find a modified form of Eq. (4) that can generate temperature data close to the analytical solution (Eq. (16)). Table 1 compares the analytical results (Eq. (16)) with the numerical results from the three energy equation cases at nine selected locations of y for $Da = 1.0$ and 0.1. Numerical data obtained in cases 2 and 3 show close agreement with the analytical data. The numerical results for case 2 is plotted in Fig. 4(a) and (b) along with the analytical results.

The simplified energy equation (Eq. (13)) expresses a balance between transverse conduction and viscous dissipation. In the limit of negligible Brinkman number ($= Ec \times Pr$) or very large Darcy number (Da), the viscous dissipation effect is negligible. In such limiting cases, the simplified energy equation reduces to a conduction equation as evidenced by the almost linear temperature profile observed at $Da = 10$. Alternatively viscous dissipation effects increase with decreasing Da, and correspondingly local fluid temperatures are seen to increase. Viscous dissipation provides a thermal energy (heat) source downstream (unlike the heat flux at the walls, which is subject to a constant-temperature bound-

Table 1
Temperature distribution at $Da = 1$, for case 1: analytical solution, case 2: numerical solution with dissipation only, case 3: numerical solution with dissipation and convection, and case 4: numerical solution with convection only

$Da = 1.0$									
	Dimensionless temperature (Θ) at								
$y =$	−1.0	−0.75	−0.50	−0.25	0.0	0.25	0.50	0.75	1.0
Case 1	0.0000	0.4065	0.7840	1.0862	1.2751	1.3362	1.2840	1.1564	1.0000
Case 2	0.0000	0.4135	0.7973	1.1040	1.2944	1.3540	1.2974	1.1635	1.0000
Case 3	0.0000	0.4135	0.7972	1.1040	1.2944	1.3540	1.2973	1.1635	1.0000
Case 4	0.0000	0.1250	0.2500	0.3750	0.5000	0.6250	0.7500	0.8750	1.0000
$Da = 0.1$									
	Dimensionless temperature (Θ) at								
$y =$	−1.0	−0.75	−0.50	−0.25	0.0	0.25	0.50	0.75	1.0
Case 1	0.0000	2.7969	5.2194	6.8691	7.5243	7.1191	5.7194	3.5469	1.0000
Case 2	0.0000	2.8527	5.3227	7.0047	7.6711	7.2548	5.8232	3.6026	1.0000
Case 3	0.0000	2.8526	5.3226	7.0045	7.6709	7.2547	5.8231	3.6026	1.0000
Case 4	0.0000	0.1250	0.2500	0.3750	0.5000	0.6250	0.7500	0.8750	1.0000

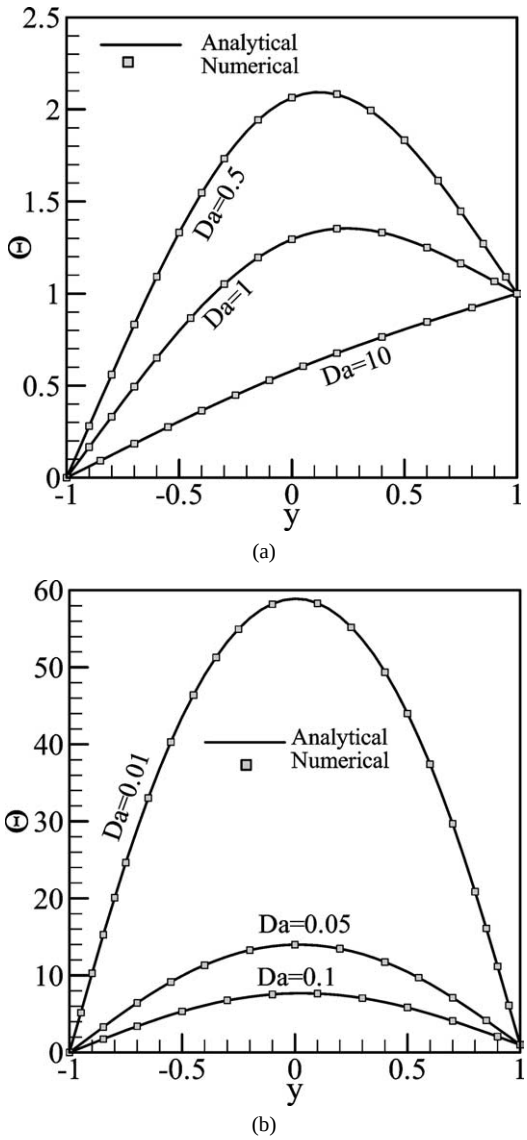

Fig. 4. (a) Temperature as a function of transverse distance at different *Da*, (b) temperature as a function of transverse distance at different *Da*.

ary condition, which decays downstream) and thus changes the nature of the fully developed temperature distribution. A decrease in Darcy number introduces a nonlinearity into the temperature profile as illustrated in Fig. 4(a) and (b); the lower the value of the Darcy number, the higher the non-linear viscous effect in the Θ–y profile. The location ($y = y_0$) of the maximum temperature inside the channel is important. As seen later, no entropy generation (HTI) occurs at the maximum temperature location since the temperature gradient is zero ($\partial\Theta/\partial y = 0$). At low Darcy number the Θ–y reveals that thermal energy (heat) is transferred to both the hot and cold plates.

5.3. Heat transfer

Heat transfer is calculated in the form of a dimensionless Nusselt number (*Nu*) using Eq. (20). The Φ–*Da* correlations given in Fig. 2 are used to calculate Φ in Eq. (20). For three selected values of Brinkman number ($Ec \times Pr =$ 0.1, 1.0, and 10), Nusselt number is plotted in Fig. 5 as a function of Darcy number for the range $10^{-3} \leqslant Da \leqslant 10^{3}$. Three distinct zones are identified in the *Nu*–*Da* profiles. In the first zone, where Darcy number is small, Nusselt number decreases linearly (on a log–log plot) with increasing Darcy number. For high Darcy numbers, Nusselt number (*Nu*) shows an asymptotic behavior for all three Brinkman numbers considered such that *Nu* approaches Nu_∞ in this zone. *Nu* asymptotes to Nu_∞ sooner (at lower value of *Da*) the smaller the Brinkman number. Between these two zones is a transition zone where the *Nu*–*Da* profile displays its only non-linear behavior. In the first and transition zones, the magnitude of the Nusselt number is higher for higher Brinkman number at a constant Darcy number.

For $Ec \times Pr = 1$, Nusselt numbers are calculated using numerical simulation at six selected values of Darcy numbers. These numerical values are compared with the analytically obtained Nusselt numbers in Fig. 5 and Table 2. The agreement between the numerical and analytical Nus-

selt numbers is good. The modified Nusselt number (Nu^*) defined by Eq. (22) is plotted in Fig. 6 as a function of Darcy number. At a very low or high permeability (i.e., $Da \to 0$ or $Da \to \infty$) of the porous media, the modified Nusselt number shows asymptotic behavior as illustrated in Fig. 6. Note that the peak of the Nu^*–Da profile, which occurs approximately at $Da \approx 0.4$, does not correspond to a heat transfer maximum; the physical meaning of Nu should not be confused with Nu^*.

Observe that a single curve (Fig. 6) illustrates the heat transfer characteristics of a multivariable problem. This

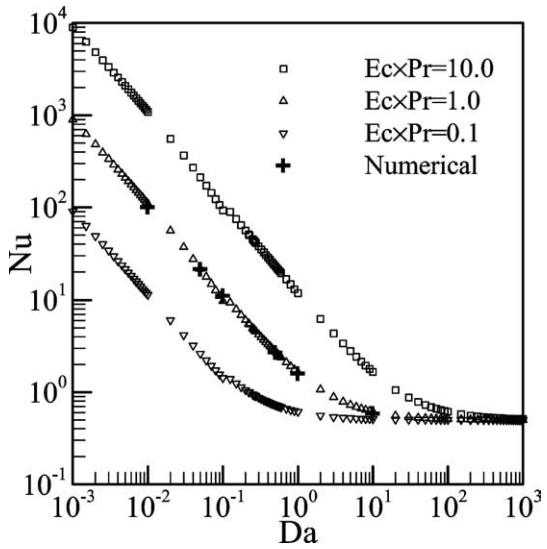

Fig. 5. Nusselt number as function of Darcy number at different Br.

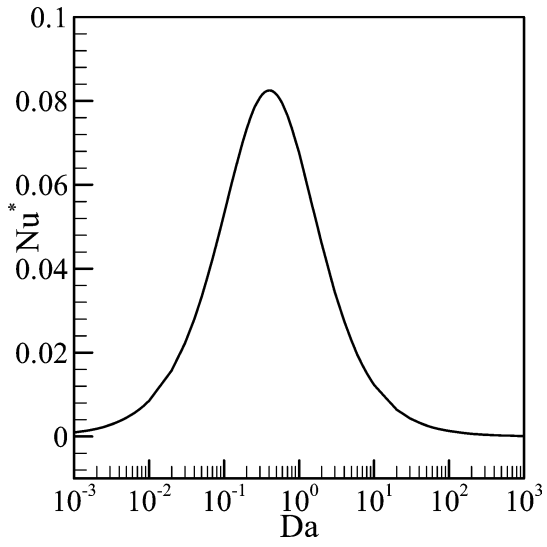

Fig. 6. Modified Nusselt number as a function of Da.

Nu^*–Da profile on a linear-logarithmic plot is Gaussian distribution like, therefore it can be expressed in a simple way as follows

$$Nu^* = b_1 \exp\left[-\frac{(Da^* - b_2)^2}{2b_3^2}\right] \tag{30}$$

where $Da^* = \log_{10}(Da)$, $b_1 = 0.08129717$, $b_2 = -0.39222124$, $b_3 = 0.69422222$. Eq. (30) is a comparatively simpler expression when compared with Eq. (22).

5.4. Entropy generation

In the case of an irreversibility analysis there are a large number of parameters to vary, and the calculations are time consuming. We have the ability to calculate the entropy generation and Bejan number fields for different combinations of the parameters considered in this paper, but in the interest of brevity we just present limited cases of local entropy generation and Bejan number distributions. In a later section we focus on their global, or average, distributions. For the special case of $Da = 1.0$, $Ec \times Pr = 1$, and $n = 1$, entropy generation number (Ns) is plotted in Fig. 7 as a function of transverse distance (y) for different group parameters (Br/Ω). The group parameter is an important dimensionless number for entropy generation analysis. It determines the relative importance of viscous effects to temperature gradient entropy generation. Entropy generation profile is asymmetric about the centerline of the channel due to the asymmetric temperature distribution. For all group parameters, each wall acts as a strong concentrator of irreversibility because of the

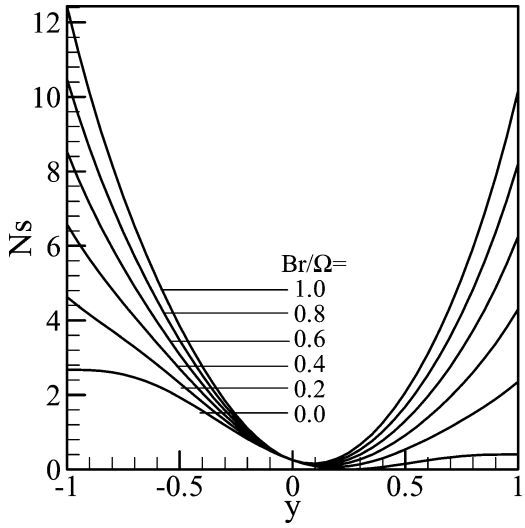

Fig. 7. Entropy generation number as a function of y at different group parameters.

Table 2
Comparison of analytical and numerical values of Nusselt number at different Darcy number ($Ec \times Pr = 1.0$)

Da	0.01	0.05	0.1	0.5	1	10
$Nu_{\text{analytical}}$	103.35	22.119	11.587	2.8083	1.6643	0.6199
$Nu_{\text{numerical}}$	99.936	21.213	11.098	2.6823	1.5849	0.5828

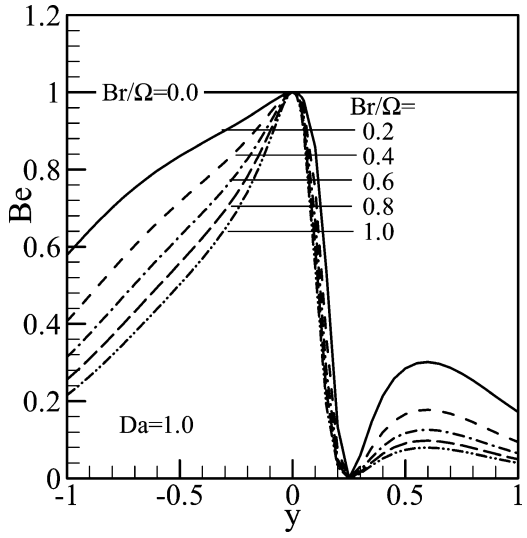

Fig. 8. Bejan number as a function of y at different group parameters.

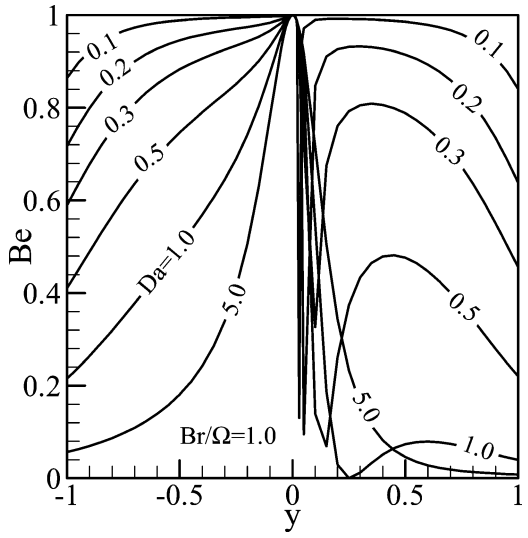

Fig. 9. Bejan number as a function of y at different *Da*.

high near-wall gradients of velocity and temperature. Maximum entropy generation occurs near the cold wall for all group parameters. Fluid friction irreversibility is zero at the channel centerline ($y = 0$) due to the zero velocity gradient ($\partial u/\partial y$). Also entropy generation number (*Ns*) is independent of group parameter at $y = 0$. Therefore, the magnitude of entropy generation rate is same at the centerline of the channel for all group parameters. Minimum entropy generation rates occur very near where the temperature gradient is zero. Except at $y = 0$, the magnitude of *Ns* is higher for higher values of the group parameter for a given location y.

5.5. Heat transfer irreversibility (HTI)

The transverse variation in heat transfer irreversibility in terms of Bejan number (*Be*) is shown in Fig. 8 at six selected group parameters. At $Br/\Omega = 0$, the contribution of fluid friction irreversibility to overall entropy generation is absent, thus resulting in an invariant distribution of Bejan number with respect to y. Bejan number shows its maximum value ($= 1.0$) for all y when $Br/\Omega = 0$. A nonzero, positive value of group parameter dramatically changes the shape of the *Be*–y profile. From the cold wall ($y = -1$) to the channel centerline ($y = 0$), the velocity gradient decreases, and the fluid friction irreversibility contributes less to overall entropy generation. Therefore, the Bejan number increases towards the channel centerline from the cold wall. Bejan number shows its maximum value ($Be = 1.0$) at $y = 0$ where there is no entropy generation due to fluid friction. Next, for a small range of transverse distance ($0 \leqslant y \leqslant 0.25$), the Bejan number rapidly drops to its minimum value ($Be = 0.0$) where the temperature gradient is zero (i.e., no contribution from HTI). Several factors influence the *Be*–y profile from the temperature maximum ($y = 0.25$) to the hot wall ($y = 1$): (a) a lower magnitude temperature gradient exists near the hot wall than the cold wall, (b) a higher velocity gradient exists near the hot wall than the centerline, similar

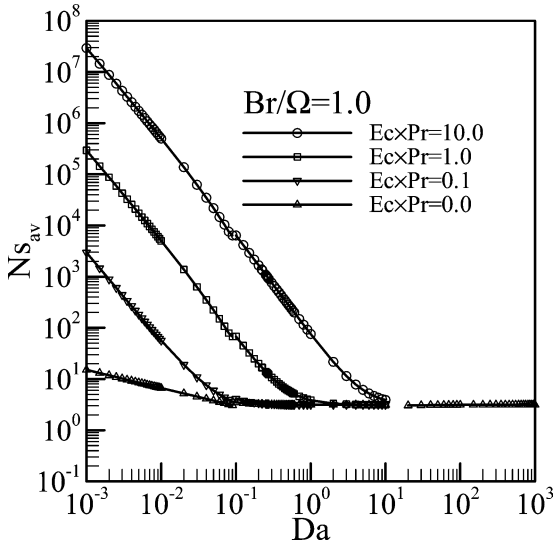

Fig. 10. Average entropy generation number as a function of *Da* at different Brinkman numbers.

to the cold wall, (c) the location of the idle point of temperature entropy generation is closer to the hot wall, etc. As a result, the Bejan number increases from its minimum value with increasing y, shows a second maximum, and then decreases towards the hot wall of the channel. Except at $y = 0$ and $y = 0.25$, an increase in group parameter strengthens the effect of fluid friction irreversibility, therefore, resulting in a lower magnitude Bejan number at a given y.

The effect of Darcy number on HTI is shown in Fig. 9. The *Be*–y profile is similar in shape to that seen in Fig. 8, and the same discussion is valid for the profiles given in Fig. 9. An increase in Darcy number strengthens the effect of fluid friction irreversibility, therefore, resulting in a lower magnitude Bejan number at a given y.

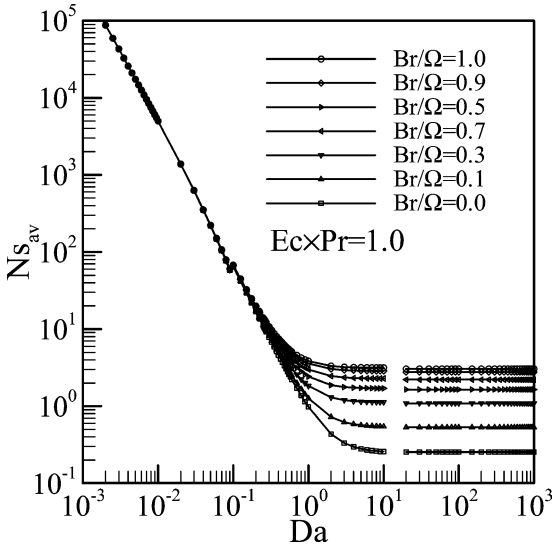

Fig. 11. Average entropy generation number as a function of *Da* at different group parameters.

5.6. Average entropy generation

From the expression for entropy generation number (Eq. (26)), the volume averaged entropy generation rate can be evaluated as follows:

$$Ns_{av} = \frac{1}{\forall}\int_{\forall} Ns\,\mathrm{d}\forall = \frac{1}{\forall}\int_z\int_y\int_x Ns\,\mathrm{d}x\,\mathrm{d}y\,\mathrm{d}z \tag{31}$$

where $\forall$ is the volume of the channel. The volume integral (Eq. (31)) reduces to a line integral for the analytical solution. For a selected range of Brinkman number, the average entropy generation number is plotted in Fig. 10 as a function of Darcy number for a constant group parameter. The average entropy generation number reveals a distribution similar to the Nusselt number distribution illustrated in Fig. 5. Depending on the value of Darcy number, three distinct zones (i.e., linear, non-linear, and asymptotic) exist in the Ns_{av}–*Da* profiles as in the *Nu*–*Da* profiles. Except in the asymptotic zone, Ns_{av} increases with increases in Brinkman number at constant Darcy number. For $Ec \times Pr = 1$ the variation of Ns_{av} with *Da* is given in Fig. 11 for seven selected group parameters where the Ns_{av}–*Da* profiles are again characterized by three distinct zones. For $Da \leqslant 0.1$ varying the group parameter does not influence the Ns_{av} distribution. The magnitude of the average entropy generation rate is higher for higher values of group parameter at the asymptotic zone illustrates in Fig. 11.

5.7. Energy streamline tracking

To understand the energy transport mechanisms inside the channel, according to Landau and Lifshitz [32], the *energy flux density vector* ($\dot{E} = \dot{E}_x\hat{i} + \dot{E}_y\hat{j}$) is calculated as follows:

$$\dot{E}_x = \rho u\left(\frac{u^2+v^2}{2} + C_pT\right) - k\frac{\partial T}{\partial x} - (u\sigma_{xx} + v\sigma_{yx})$$

$$\dot{E}_y = \rho v\left(\frac{u^2+v^2}{2} + C_pT\right) - k\frac{\partial T}{\partial y} - (u\sigma_{xy} + v\sigma_{yy}) \tag{32}$$

where the stress components, σ_{xx}, σ_{yy}, σ_{xy}, and σ_{yx} are be defined as

$$\sigma_{xx} = \frac{2\mu}{3}\left[2\frac{\partial u}{\partial x} - \frac{\partial v}{\partial y}\right]$$

$$\sigma_{yy} = \frac{2\mu}{3}\left[2\frac{\partial v}{\partial y} - \frac{\partial u}{\partial x}\right]$$

$$\sigma_{xy} = \sigma_{yx} = \mu\left[\frac{\partial u}{\partial y} + \frac{\partial v}{\partial x}\right] \tag{33}$$

The magnitude of the *energy flux density vector* is the amount of energy passing, in unit time, through a unit area perpendicular to the direction of fluid velocity (Landau and Lifshitz [32]). At any particular space location (for example, $P(x_0, y_0)$) inside the channel, $\dot{E}$ of that location is tangent to the energy streamline passing through the point $P(x_0, y_0)$. The energy streamline should not be confused with the heatline (Bejan [2]) which is a graphical way to interpret the heat function (the concept of heat function uses thermal diffusion and enthalpy flow together with some mathematical operations [2]). A 2-D channel of aspect ratio 15 (length/width) is chosen to show the characteristics of the energy streamline. The choice of an aspect ratio of 15 is arbitrary. The resulting energy streamline is presented in Fig. 12(a)–(e) for four selected Darcy numbers. At $Da = 0.001$ (Fig. 12(a)) the channel inlet acts as an energy 'source'. Energy flows from the inlet to the top and bottom walls with each wall behaving similar to a 'sink' of energy. A very low permeability is responsible for a very high dissipation of energy inside the channel, thus causing a rise in the fluid temperature and hence the thermal energy. Low permeability is also responsible for a slower motion of the fluid resulting in a reduction in kinetic energy. Increasing amounts of energy leave the channel via the walls at lower *Da*; the maximum in Fig. 12 being for the lowest *Da* shown ($Da = 0.001$).

The energy streamline at $y = 0$ for $Da = 0.001$ passes through the channel effectively without perturbation. This mid-streamline of energy divides the channel into two symmetrical parts having similar energy streamline distribution patterns, even though the temperatures at the top and bottom walls are not equal.

An asymmetric energy streamline distribution is seen at $Da = 0.01$ (Fig. 12(b)) with energy streamlines being perturbed a little near the inlet section of the channel. This near inlet perturbation of the energy streamline increases with increasing *Da*. At $Da = 1.0$ (Fig. 12(c)), part of the hot wall acts as an energy source. Two effects are significant at this Darcy number: comparatively (a) a high permeability of the porous media and (b) a low dissipation rate. Near the inlet section, where both the velocity and temperature distributions are developing, thermal energy transfers from the initial portion of the hot wall to the fluids. The magnitude of the velocity increases along the axial direction in the developing region, thus resulting in an increase in kinetic energy. At the same time thermal energy increases by

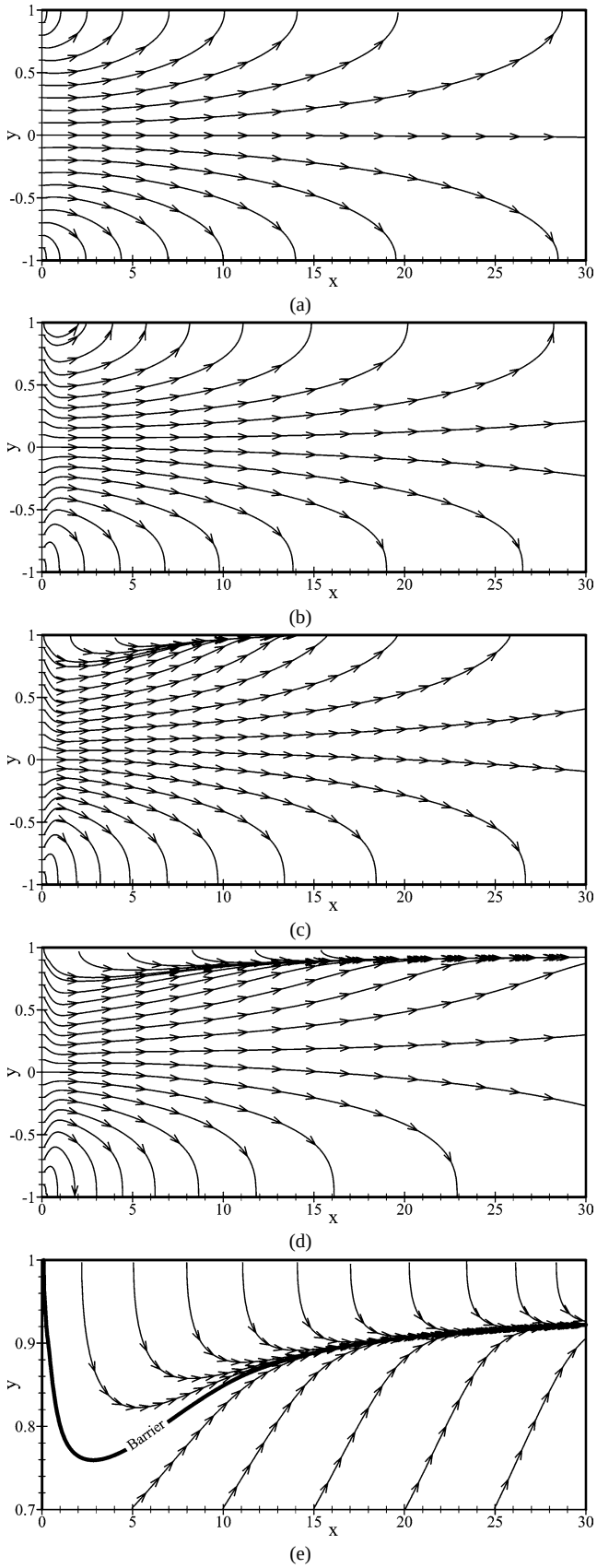

Fig. 12. Distribution of energy streamlines at (a) $Da = 0.001$, (b) $Da = 0.01$, (c) $Da = 1.0$, (d) $Da = 1000$, and (e) magnified view of the upper portion of Fig. 12(d).

viscous dissipation inside the channel. Increasing kinetic energy and thermal energy strengthens the energy source inside the media, therefore forcing the energy streamlines towards the hot wall further downstream. For the hot wall, the location $x = 14.6$ acts as a neutral point dividing the hot wall into a source and a sink. In contrast, the behavior of the bottom wall remains unchanged. As Darcy number increases, the neutral point moves to the right, thus shortening the sink-length at the hot wall until the entire top hot wall behaves as an energy source. It is difficult to determine the exact value of Darcy number that locates the neutral point at the outlet of the channel, thus it is left for future work.

Fig. 12(d) shows the energy streamlines for $Da = 1000$. A magnified view of the upper portion of the channel is shown in Fig. 12(e). The *barrier* (heavy solid line without an arrow) is a special energy streamline that originates at the intersection of the inlet and the hot wall. All energy streamlines between the barrier and hot wall originate from the hot wall (the hot wall acts as an energy source along it entire length at $Da = 1000$), and then merge with the barrier, leaving the channel following the path of the barrier. For these energy streamlines the barrier is simply an *energy corridor*. A significant portion of energy streamlines at the bottom of the barrier shows the similar characteristics of leaving the channel.

5.8. Modifications required for thermoacoustic problem

Section 5.7 completes our analyses of porous stack in the steady-state limit. To modify the present problem to a thermoacoustic problem, the unsteady terms, $\partial u/\partial \tau$ and $\partial v/\partial \tau$, should be added to the x-momentum (Eq. (2)) and y-momentum (Eq. (3)) equations, respectively. The energy equation should be modified by adding the following terms: $\partial \Theta/\partial \tau$ and $Dp/D\tau$, respectively. A standard perturbation expansion [3,4] is required in order to generate the governing equations for small-amplitude thermoacoustic variables (velocity, temperature, etc.). The wave equation should be modeled using the continuity and momentum equations in order to provide an expression for pressure. Once the solutions for velocity, temperature, and pressure are available, one can calculate Nusselt number, entropy generation number, Bejan number, and energy flux density using the appropriate equations given in this paper. The non-porous thermoacoustic formulation for a single plate and channel by Mahmud and Fraser [33,34] gives a good sense of the scope of understanding the complicated thermoacoustic problems' modeling.

6. Conclusions

Darcy number is an important dimensionless parameter for the present study as it represents a relative measure of the permeability of the porous media studied. For two limiting cases of Darcy number, $Da \to 0$ and $Da \to \infty$, the velocity profile approaches a slug-flow profile and a plane Poiseuille

flow profile, respectively. For intermediate values of Darcy number, velocity profiles are characterized by a high near wall velocity gradient and a flat profile near the center of the channel. Both the flatness of the profile near the center and the velocity gradient near the wall decrease with increasing Darcy number. For high Darcy number, a conduction like temperature profile is obtained. However, for moderate and low Darcy numbers, the fluid inside the channel is heated by viscous dissipation consequently a non-linear distribution in temperature is observed. Both Nusselt number and average entropy generation number show similar distribution characteristics. At low Darcy numbers Nu and Ns_{av} reveal a linear variation with Da on a log–log plot. Next, a non-linear variation of Nu and Ns_{av} with Da is observed at moderate Darcy numbers followed by asymptotic behavior at high Darcy numbers. The value of Darcy number, where an asymptotic behavior of Nu and Ns_{av} starts, is sensitive to the magnitude of Brinkman number ($Ec \times Pr$) with asymptotic behavior starting earlier for smaller Brinkman number. For some special cases, analytical results of velocity, temperature, and Nusselt number are compared with the results obtained from numerical simulation. For each case, good agreement between analytical and numerical results is obtained. For all Darcy numbers the cold wall act as an energy sink whereas the hot wall behaves as an energy source at small Darcy numbers. However, at moderate Darcy numbers, the hot wall acts as a combination of an energy source and an energy sink, with the dividing neutral point moving towards the outlet of the channel with increasing Da.

References

[1] D.A. Nield, A. Bejan, Convection in Porous Media, Springer, New York, 1992.
[2] A. Bejan, Convection Heat Transfer, Wiley, New York, 1984.
[3] G.W. Swift, Thermoacoustics: A Unifying Perspective for Some Engines and Refrigerators, ASA Publication, New York, 2002.
[4] N. Rott, Thermoacoustics, Adv. Appl. Mech. 20 (1980) 135–175.
[5] G.W. Swift, Thermoacoustic engines, J. Acous. Soc. America 84 (1988) 1145–1180.
[6] M. Kaviany, Laminar flow through a porous channel bounded by isothermal parallel plates, Internat. J. Heat Mass Transfer 28 (1985) 851–858.
[7] K. Vafai, S.J. Kim, Forced convection in a channel filled with a porous medium: An exact solution, J. Heat Transfer 111 (1989) 1103–1106.
[8] D.A. Nield, S.L.M. Junqueira, J.L. Lage, Forced convection in a fluid-saturated porous-medium channel with isothermal or isoflux boundaries, J. Fluid Mech. 322 (1996) 201–214.
[9] D. Poulikakos, K. Renken, Forced convection in a channel filled with porous medium, including the effects of flow inertia, variable porosity, and Brinkman friction, J. Heat Transfer 109 (1987) 880–888.
[10] K. Renken, D. Poulikakos, Experiment and analysis of forced convective heat transport in a packed bed of spheres, Internat. J. Heat Mass Transfer 31 (1988) 1399–1408.
[11] A. Nakayama, H. Koyama, F. Kuwahara, Analysis on forced convection in a channel filled with a Brinkman–Darcy porous medium: Exact and approximate solutions, Heat Mass Transfer 23 (1988) 291–295.
[12] D.A. Nield, A.V. Kuznetsov, M. Xiong, Thermally developing forced convection in a porous medium: parallel plate channel or circular tube with walls at constant temperature, J. Porous Media 7 (2004) 19–27.
[13] D.A. Nield, A.V. Kuznetsov, M. Xiong, Thermally developing forced convection in a porous medium: parallel plate channel or circular tube with walls at constant heat flux, J. Porous Media 6 (2003) 203–212.
[14] D.A. Nield, A.V. Kuznetsov, M. Xiong, Thermally developing forced convection in a porous medium: Parallel plate channel with walls at uniform temperature, with axial conduction and viscous dissipation effects, Internat. J. Heat Mass Transfer 46 (2003) 643–651.
[15] A. Hadim, Forced convection in a porous channel with localized heat sources, J. Heat Transfer 116 (1994) 465–472.
[16] H.J. Sun, S.Y. Kim, J.M. Hyun, Forced convection from an isolated heat source in a channel with porous medium, Internat. J. Heat Fluid Flow 16 (1995) 527–535.
[17] C. Cui, X.Y. Huang, C.Y. Liu, Forced convection in a porous channel with discrete heat sources, J. Heat Transfer 123 (2001) 404–407.
[18] D.A. Nield, Effects of local thermal nonequilibrium in steady convective processes in a saturated porous medium: Forced convection in a channel, J. Porous Media 1 (1998) 181–186.
[19] D.A. Nield, A.V. Kuznetsov, Local thermal nonequilibrium effects in forced convection in a porous medium channel: A conjugate problem, Internat. J. Heat Mass Transfer 42 (1999) 3245–3252.
[20] G. Chen, H.A. Hadim, Forced convection of a power-law fluid in a porous channel—numerical solutions, Heat Mass Transfer 34 (1998) 221–228.
[21] A. Bejan, Entropy Generation Minimization, CRC Press, New York, 1996.
[22] A. Bejan, Fundamental of exergy analysis, entropy generation minimization, and the generation of flow architecture, Internat. J. Energy Res. 26 (2002) 545–565.
[23] A. Bejan, G. Tsatsaronis, M. Moran, Thermal Design and Optimization, Wiley, New York, 1996.
[24] K. Vafai, C.L. Kim, Analysis of surface enhancement by a porous substrate, J. Heat Transfer 112 (1990) 700–706.
[25] M.L. Hunt, C.L. Tien, Effects of thermal dispersion on forced convection in fibrous media, Internat. J. Heat Mass Transfer 31 (1988) 301–309.
[26] S. Mahmud, P.K. Das, N. Hyder, A.K.M.S. Islam, Free convection in an enclosure with vertical wavy walls, Internat. J. Thermal Sci. 41 (2002) 440–446.
[27] F.M. White, Viscous Fluid Flow, McGraw-Hill, New York, 1991.
[28] D.A. Nield, Resolution of a paradox involving viscous dissipation and nonlinear drag in a porous medium, Transport in Porous Media 41 (2000) 349–357.
[29] A.K. Al-Hadhrami, L. Elliott, D.B. Ingham, A new model for viscous dissipation in porous media across a range of permeability values, Transport in Porous Media 53 (2003) 117–122.
[30] A. Bejan, Convection Heat Transfer, Wiley, New York, 1984.
[31] S.H. Tasnim, S. Mahmud, M.A.H. Mamun, Entropy generation in a porous channel with hydromagnetic effect, Exergy 2 (2002) 300–308.
[32] L.D. Landau, E.M. Lifshitz, Fluid Mechanics, Gopsons, Noida, 2003.
[33] S. Mahmud, R.A. Fraser, Viscous oscillatory flow inside stacks: Non-conjugate formulation, in: Proc. 2nd BSME–ASME Int. Conf. Thermal Engrg., Dhaka, 2–4 January 2004.
[34] S. Mahmud, R.A. Fraser, A single plate thermoacoustic system: Viscous conjugate problem, in: Proc. Int. Conf. Mechanical Engrg., ICME 2003, Dhaka, 26–28 December 2003.